HAL
open science

Direct U-Pb dating of carbonates from micron scale fsLA-ICPMS images using robust regression

Guilhem Hoareau, Fanny Claverie, Christophe Pécheyran, Christian Paroissin, Pierre-Alexandre Grignard, Geoffrey Motte, Olivier Chailan, Jean-Pierre Girard

To cite this version:

Guilhem Hoareau, Fanny Claverie, Christophe Pécheyran, Christian Paroissin, Pierre-Alexandre Grignard, et al.. Direct U-Pb dating of carbonates from micron scale fsLA-ICPMS images using robust regression. Geochronology Discussion, 2021, 3, pp.67-87. 10.5194/gchron-3-67-2021 . hal-02898238

HAL Id: hal-02898238

https://hal.science/hal-02898238v1

Submitted on 13 Jul 2020

HAL is a multi-disciplinary open access archive for the deposit and dissemination of scientific research documents, whether they are published or not. The documents may come from teaching and research institutions in France or abroad, or from public or private research centers.

L'archive ouverte pluridisciplinaire **HAL**, est destinée au dépôt et à la diffusion de documents scientifiques de niveau recherche, publiés ou non, émanant des établissements d'enseignement et de recherche français ou étrangers, des laboratoires publics ou privés.

https://doi.org/10.5194/gchron-2020-10
This is just a preview and not the published preprint.
© Author(s) 2020. CC-BY 4.0 License.

Direct U-Pb dating of carbonates from micron scale fsLA-ICPMS images using robust regression

Guilhem Hoareau[1], Fanny Claverie[2], Christophe Pecheyran[2], Christian Paroissin[3], Pierre-Alexandre Grignard[1], Geoffrey Motte[1], Olivier Chailan[4] and Jean-Pierre Girard[4]

[1] Universite de Pau et des Pays de l'Adour, E2S UPPA, CNRS, TOTAL, LFCR, UMR5150, 64000 Pau, France
[2] Universite de Pau et des Pays de l'Adour, E2S UPPA, CNRS, IPREM, UMR5254, 64000 Pau, France
[3] Universite de Pau et des Pays de l'Adour, E2S UPPA, CNRS, LMAP, UMR5142, 64000 Pau, France
[4] TOTAL, CSTJF, F-64018 Pau Cedex, France

Correspondence to: Guilhem Hoareau (guilhem.hoareau@univ-pau.fr), Christophe Pécheyran (christophe.pecheyran@univ-pau.fr)

Abstract. U-Pb dating of carbonates by LA-ICPMS spot analysis is an increasingly used method in the field of geosciences, as it brings very strong constraints over the geological history of basins, faults or reservoirs. Most ages currently published are based on the measurement of U and Pb ratios on spot ablations, using nanosecond lasers coupled to sector-field or multi-collector ICPMS. Here, we present a new strategy for the U-Pb dating of carbonates from 2D isotopic ratio maps, based on the use of a robust regression approach in the data reduction workflow. The isotopic maps, having minimum area of 0.65 mm^2 (~1000 pixels of 13x25 µm resolution), are obtained using a 257 nm femtosecond laser ablation system at high repetition rate (500 Hz) coupled to a High Resolution ICPMS. The maps commonly show significant variations in isotope ratios at the pixel scale, allowing the plotting of pixel U-Pb ratios in concordia or isochron diagrams and the calculation of U-Pb ages. Due to the absence of individual ratio uncertainties, the ages are calculated by using MM-robust linear regression rather than the more commonly used York-type regression. Provided examples demonstrate that this strategy allows calculating ages and uncertainties similar to those obtained for samples already dated by more traditional techniques (isotope dilution or LA-ICPMS spot analyses). The goodness-of-fit to the data is assessed by the calculation of the residual standard error of the regression (RSE), and by the calculation of a MSWD on discretized data. The regression method proposed is a statistically robust, alternative approach to that proposed by Drost et al. (2018), that can be easily applied to U-Pb age determination from isotopic maps.

1 Introduction

Since the seminal publication of Li et al. (2014), the U-Pb dating of carbonates by LA-ICPMS has progressed significantly with applications as varied as the dating of tectonic fractures and veins (e.g., Roberts & Walker, 2016; Beaudoin et al., 2018; Parrish et al., 2018; Nuriel et al., 2019), carbonate deposition (Drost et al., 2018), speleothems (Woodhead et al., 2019) or

https://doi.org/10.5194/gchron-2020-10
This is just a preview and not the published preprint.
© Author(s) 2020. CC-BY 4.0 License.

cements filling the porosity of reservoirs (e.g., Li et al., 2014; Godeau et al., 2018). This is due, among other benefits, to the very good spatial resolution of the method, which allows dating minerals with a surface area of less than one millimeter, to its quickness, allowing to date several samples per day, as well as to the recent availability of carbonate standards to correct matrix-related offsets of U/Pb ratios (Roberts et al., 2017). Given the ubiquitous nature of carbonates, the technique is likely to be associated with a growing number of studies in the future (Roberts et al., 2019).

The vast majority of carbonate dating LA-ICPMS studies are based on spot ablations of sizes close to 100 µm, where isochrones can be constructed from the combination of several tens of ablation craters made on the same crystal or, by default, on adjacent crystals when their size is too small (e.g. micrite). There is now enough hindsight on the applicability of the method to show that this approach allows precise ages to be obtained (< 3% in the most favourable cases) (Roberts et al., 2019). In addition, the fact that most ablation cells can accommodate multiple samples simultaneously makes it possible to automatically analyze multiple samples per session, including primary and secondary standards. As recently recalled by Roberts et al. (2019), the heterogeneous nature of carbonates requires, however, prior petrographic and preferably geochemical characterization of the samples to maximize the chances of successful dating. An initial screening of samples by LA-ICPMS to produce images of diagnostic trace element concentrations seems to be a particularly adapted method to localize U-rich and unaltered zones, in which precise and meaningful ages can be obtained (Roberts et al., 2019).

An alternative carbonate dating method based on age extraction from LA-ICPMS maps was recently presented by Drost et al. (2018). As before, the simultaneous analysis of many trace elements (including of course U and Pb isotopes) allows visualizing the most favourable areas for dating. However, in this case, the concentrations of elements characteristic of detrital contamination (e.g., Zr, Rb etc) are used to define pixel exclusion thresholds, thus filtering out the values corresponding, most likely, to microscopic inclusions of other minerals (e.g., clays). The isotopic U and Pb values of the remaining pixels are used to build isotopic ratio maps, from which a U-Pb age can be calculated. The methodology of age determination proposed by these authors is based on the sorting of pixel ratio values used in dating ($^{238}U/^{206}Pb$, $^{207}Pb/^{206}Pb$ for a Tera-Wasserburg (TW) diagram) based on $^{238}U/^{208}Pb$ and $^{235}U/^{207}Pb$ pixel ratios and their pooling (i.e., discretization) to subsets ('pseudo-analyses') of similar number of pixels for which the mean values and associated standard errors (i.e., standard deviations of the mean) are calculated. These values are then plotted in TW, 86TW ($^{208}Pb_{common}/^{206}Pb$ versus $^{238}U/^{206}Pb$; Parrish et al., 2018) and isochron diagrams ($^{206}Pb/^{208}Pb_{common}$ versus $^{238}U/^{208}Pb_{common}$) to calculate the age using York-type regressions as implemented in Isoplot (Ludwig, 2012) or IsoplotR (Vermeesch, 2018). Additional examples of the interest of this new approach are provided in Roberts et al. (2019).

In this contribution, we propose a simple, alternative approach for the calculation of U-Pb carbonate ages from isotopic maps. Rather than the pooling of pixel values proposed by Drost et al. (2018), the pixel isotopic ratios of interest are directly plotted in the concordia or isochron diagrams, and a statistically robust linear regression that is extremely robust to outliers is processed through the pixels to obtain the age. The visualization of all pixel ratio values in the TW or isochron diagrams allows the user to assess visually the quality of data, guided by a more common statistical parameter such as the residual standard error (RSE). Discretization is also used to calculate pseudo-MSWD values that permit assessing the linearity of pixel data. The robust

https://doi.org/10.5194/gchron-2020-10
This is just a preview and not the published preprint.
© Author(s) 2020. CC-BY 4.0 License.

regression method appears to be ideally suited to isotopic maps obtained after pixel filtering based on trace element concentrations or, as proposed here, pixel colocalization study.

2 Method

2.1 Choice of samples

Four samples of already dated lacustrine and reefal carbonates, and tectonic veins have been chosen to demonstrate the usefulness of the robust regression approach. The samples are

(i) a lacustrine limestone Long Point (Duff Brown Tank locality in the Colorado Plateau, USA), precisely dated by Hill et al. (2016) at 64.04 ± 0.67 Ma (2s) by U-Pb methods using isotope dilution (ID) MC-ICPMS, and labelled Duff Brown in the following. This sample serves as a secondary standard in the analytical procedure and has also been demonstrated to be suitable for U-Pb dating using image maps by Drost et al. (2018);

(ii) a tectonic calcite vein (BH14) from the Bighorn basin (Wyoming, USA) dated by U-Pb LA-ICPMS spot analyses (i.e., range of spot ablations) at 63 ± 2.2 Ma by Beaudoin et al. (2018) and at 61 ± 2.9 Ma in our laboratory (the detailed methodology is presented in the Supplementary Material), with the same calcite standards as the present study (WC1 and Duff Brown);

(iii) a reefal limestone sample from the southern Pyrenees (PXG20-1), located in the upper part of the Pamplona marls in the Atarés anticline. This sample has been dated at 40.5 ± 2.3 Ma in our laboratory by LA-ICPMS spot analysis. A micropaleontologic study from Canudo and Molina (1988) performed close to the sampling area suggests an upper Bartonian to Priabonian age for the deposits (~38.5-36 Ma), whereas the paleomagnetic study of Oms et al. (2003) are more consistent with a Bartonian age (~40-38.5 Ma);

(iv) a lacustrine carbonate from the southern Pyrenees (PXG32-2), which is part of the first continental deposits of the Campodarbe Formation flanking the western limb of the Boltana anticline (eastern Jaca basin). Previous magnetostratigraphic and tectono-sedimentary studies point to a Bartonian-Priabonian age of deposition (Mochales et al., 2016). A similar age was obtained by U-Pb LA-ICPMS spot analysis, although with a poor statistic (37 ± 3 Ma; MSWD = 6.3).

Two additional undated samples of calcite cements found in tectonic breccias and veins affecting Tithonian limestones of the northern Pyrenees (France) are also presented (ETC2 and ARB). They provide examples of application of the technique to the resolution of the diagenetic evolution of areas with complex tectonic evolution.

https://doi.org/10.5194/gchron-2020-10
This is just a preview and not the published preprint.
© Author(s) 2020. CC-BY 4.0 License.

2.2. Analytical strategy

2.2.1. LA-ICPMS instrumentation

All the samples were analyzed with a femtosecond laser ablation system (Lambda3, Nexeya, Bordeaux, France) coupled to an HR-ICPMS Element XR (ThermoFisher Scientific, Bremen, Germany) fitted with the Jet Interface. The laser is fitted with a diode-pumped Yb:KGW crystal laser source (HP2, Amplitude Systèmes, Pessac, France). The pulse duration is less than 400 fs at 257 nm. The laser source can operate within a wide range of repetition rates (1 Hz to 100 kHz) and energy ranging from 200 µJ per pulse below 1 kHz to 1 µJ at 100 kHz at 257 nm. Complex trajectories can be realized by moving the laser beam (15 µm diameter at full energy) across the surface of the sample using the rapid movement of galvanometric scanners combined with a high repetition rate (Ballihaut et al., 2007, Aramendia et al., 2015) (Fig. 1A).

The aerosol produced by the ablation was carried to the ICP-MS by a tube (1/16" internal diameter) using an Helium stream (600 mL min^{-1}, with exception for the first session in October 2018, where argon was used (650-700 mL min-1)). Measured wash out time of the ablation cell was ~500 ms for helium gas and ~1 s for argon gas considering the 99% criterion. To improve sensitivity, 10 mL min^{-1} of nitrogen was added to the helium flow before mixing with argon in the ICP-MS. Measurements were performed under dry plasma conditions. The fs-LA-ICP-MS coupling was tuned on a daily basis in order to achieve the best compromise in terms of sensitivity, accuracy, particles atomization efficiency and stability. The additional Ar carrier gas flow rate, torch position and power were adjusted so that the U/Th ratio was close to 1 +/- 0.05 when ablating the glass SRM NIST612. Detector cross-calibration and mass bias calibration were checked daily using the appropriate sequence of the Element Software. The laser and HR-ICPMS parameters used for U-Pb dating are detailed in Annex A. Only ^{238}U, ^{232}Th, ^{208}Pb, ^{207}Pb, and ^{206}Pb were selected, reaching a total mass sweep times of about ~60 ms. The analysis of trace elements with lower atomic masses, in a purpose of pixel selection as done by Drost et al. (2018) was not attempted due to the inability of the sector-field ICPMS to achieve reasonable total mass sweep times (due to magnet mass change).

2.2.2. Analytical workflow

Two types of isotopic maps were produced:

(i) The first one was designed to identify the most favourable areas for dating (high U/Pb), over a large surface of the sample. In this configuration, samples were first ablated along lines of 6.5 to 7.8 mm length at a repetition rate of 300 Hz. The lines of 50 µm width were obtained using a back and forth movement of the laser (at 10 $mm.s^{-1}$) combined with a stage movement rate of 100 $\mu m.s^{-1}$ (Fig. 1A), corresponding to 64.5 to 78 s of analysis per line, followed by 15 seconds of break between the lines (to allow ICPMS data processing). The lines were separated by a distance of 100 µm. The number of lines was of 40 to 56, resulting in a duration of 53 to 78 minutes for a complete map of surface comprised between 26 and 38.1 mm^2. The maps produced are presented in Figure S2.

(ii) The second one was designed to date the samples. Therefore, they were performed in selected area (from map 1) and consisted in linear scans of 0.8 to 1.6 mm length at a repetition rate of 500 Hz. These lines of 25 µm width, separated

https://doi.org/10.5194/gchron-2020-10
This is just a preview and not the published preprint.
© Author(s) 2020. CC-BY 4.0 License.

by a distance of 25 µm, were obtained using a back and forth movement of the laser (at 5mm.s^{-1}) combined with a stage movement rate of 25 µm.s^{-1}, corresponding to 32 to 64 s of analysis per linear scan, followed by 15 seconds of break. The number of lines was of 25 to 27, resulting in a total analysis time ranging from 19 to 38 minutes for a complete map of surface comprised between 0.5 and 1.1 mm^2 (Fig. 1B). Before analysis, the samples were pre-cleaned with the laser using a stage movement rate of 200 µm.s^{-1}. The unknowns were bracketed with the SRM NIST612 for lead ratios, followed by the commonly used WC1 calcite standard (Age 254.4 ± 7 Ma; Roberts et al. (2017)) for the Pb/U ratio, using the standardization method of Roberts et al. (2017). Two unknowns could be analysed in a row between the standards. The standards were analysed in conditions similar to the unknowns, except that the isotopic maps were of smaller surface (~0.2 mm^2), corresponding to an analysis time of ~5 minutes. The ablation depth was comprised between ~25 µm and ~35 µm.

2.3. Data processing and uncertainty propagation workflow

2.3.1. Construction of isotopic maps and blank correction

For each map, the first line corresponds to the ICPMS signal recorded without laser ablation in order to calculate average blank values for the different masses. The matrices of raw isotopic values (in counts per seconds) were then built using a home-made python code including blank correction (subtraction of average blank for each data point). Visualization as maps were processed with the Fiji freeware. All isotopic maps are imported as an image stack and appropriately cropped. To consider the wash-out time, the number of pixels was averaged by 8 along each linear scan in order to reach a value of one pixel per 500 ms and 1000 ms for He and Ar, respectively. The isotopic ratio matrices were then calculated.

2.3.2. Normalization of the Pb/Pb and U/Pb isotopic ratios

For the glass SRM NIST612, Pb (and U) isotopic ratios were calculated as the robust mean of the ratios over the entire image, using the "Huber" function of the *Statsmodels* Python library. The robust mean is obtained through an iterative process that uses a Huber loss function to strongly reduce the weight of any outlier (i.e., spike) onto the final result, without any manual outlier rejection. The Pb isotopic ratios of the glass SRM NIST612 standard were used to normalize the pixel ratios of the WC1 and unknown sample images, by standard bracketing. The standard error (i.e., standard deviation of the mean) for each ratio was also calculated from the standard deviation which is an output of the function.

For WC1 calcite, an age was calculated from the combination of both isotopic maps that bracket the unknown sample. The age, obtained with the robust regression method described in detail below was used to calculate the correction factors for the U/Pb ratios, following the approach of Roberts et al (2017). The correction factor was calculated for a TW regression, with the ^{207}Pb/^{206}Pb anchored to a value of 0.85 as determined from isotope dilution methods (Roberts et al., 2017). The U/Pb isotopic ratios of all pixels of the unknown sample isotopic maps were corrected by the obtained correction factor.

https://doi.org/10.5194/gchron-2020-10
This is just a preview and not the published preprint.
© Author(s) 2020. CC-BY 4.0 License.

2.3.3. Age calculation of the unknown

All regressions were performed using a statistically robust linear regression approach based on a Tukey bi-weight loss function. All the pixel isotopic values were first plotted in the appropriate plot (TW, 86TW and isochron plots). The regression was then made using the *lmrob* package in R (Maechler et al, 2019). In the chosen setting (*KS2014*) the package allows to automatically perform an MM-robust regression, which has a high breakdown efficiency and is demonstrated to be highly efficient against outliers (Koller and Stahel, 2011, 2017). Based on an iterative process, the method automatically attributes a weight to each point, with lowest weights corresponding to the outliers. The final regression is then a weighted linear fit through the points. In our procedure, a second step of robust regression is done after rejection of 2.5% of points (i.e., above 2.3 sigma outliers). Finally, the age calculation used the classical geochronological equations, corresponding to the lower intercept of the regression line with the concordia in the TW space, with the x-axis in the TW86 space, and to the slope of the regression line in the isochron diagram.

2.3.4. Uncertainties

In the commonly used York-type weighted linear regressions, the weight of each point is inversely proportional to its uncertainty (i.e., size of the ellipse), where the latter commonly corresponds to the quadratic addition of analytical uncertainties (Horstwood et al., 2016). In contrast, the pixel isotopic ratios used for the robust regression have no uncertainty, as they are directly calculated from the number of counts of the relevant masses. All uncertainties (analytical or systematic) were therefore added quadratically to the age uncertainty obtained from the confidence interval of the robust regression. Following recommendations of Horstwood et al. (2016), these uncertainties were added to the U/Pb ratio uncertainty corresponding to the age, rather than to the age uncertainty itself. The analytical uncertainties considered are those calculated for the homogeneous primary standard (glass SRM NIST612). The systematic uncertainties are the decay constant uncertainty of ^{238}U (0.05%, 1s), and the $^{238}U/^{206}Pb$ ratio uncertainty of WC1, as estimated by Roberts et al. (2017) (1.35%, 1s). Note that the long-term excess variance of the NIST612 standard will be added as additional systematic uncertainty in future studies (e.g., Horstwood et al., 2016).

2.3.5. Estimation of the goodness-of-fit

In geochronology, the parameter usually most used in the estimation of goodness of fit is the Mean Square of Weight Deviates (MSWD), or reduced chi-squared, whose value close to 1 is interpreted as a strong indication of the quality of the regression. The calculation of the MSWD can, by definition, only be performed from values associated with uncertainties, which is not the case for the points used for the robust regression. Two steps have been adopted in this work to quickly assess the goodness of fit of the robust regressions. The first one is the calculation of the F-test of overall significance. If the F-test is higher than the significance level (chosen at 0.05), the regression is rejected and the dating considered unsuccessful. In case of success of this first step, the second one considers several parameters that help assessing the quality of the regression. One parameter is

https://doi.org/10.5194/gchron-2020-10
This is just a preview and not the published preprint.
© Author(s) 2020. CC-BY 4.0 License.

the Residual Standard Error (RSE) of the robust regression, an output of the *lmrob* method, which provides an estimate of the mean dispersion of the points around the regression in absolute value of the y-axis. The smaller the RSE, the smaller the dispersion. An additional approach used to estimate the goodness of fit is the calculation of an MSWD from a discretization of the points used for regression, which we call d-MSWD. Here the points are discretized into sets classified by increasing U/Pb ratios (i.e., $^{238}U/^{206}Pb$ for the TW and 86TW diagrams or $^{238}U/^{208}Pb_{common}$ for the isochrone diagram). For each set, the number of points always corresponds to the equivalent of 30 seconds of analysis (i.e. 60 pixels for He and 30 pixels for Ar), which is the most common duration of laser ablations in spot LA-ICPMS studies. The weighted mean and standard error of the sets are calculated (i.e. ellipses). The calculation of the d-MSWD is performed by considering the robust regression obtained previously, and a d-MSWD value close to 1 is expected for points (here sets) well aligned along the regression. This approach is close to the one used by Drost et al. (2018) for their age calculations, except that discretization is not performed using the $^{235}U/^{207}Pb$ or $^{238}U/^{208}Pb$ ratios, the MSWD is not based on the use of York-type regression, and the number of pixels per ellipse is not adjusted opportunely for each sample to tend toward better MSWD value. In parallel with the calculation of the d-MSWD, a TW plot with the corresponding ellipses, as well as a representation of the running mean with 60 and 30 pixels for He and Ar, respectively, is also systematically produced to assist in the user's assessment of the quality of the point alignment and thus the validity of the linear regression.

2.3.6. Colocalization study

The lack of trace element concentration data prevents the adoption of a pixel selection approach as presented by Drost et al. (2018). In order to select the most favourable areas of the isotope maps to obtain precise ages, a pixel value colocalization approach using the ImageJ plugin ScatterJn (Zeitvogel and Obst, 2016) was used. The pixel values of the $^{207}Pb/^{206}Pb$ and $^{238}U/^{206}Pb$ isotopic maps were plotted in a TW scatterplot, and areas selected in the spatial domain (maps) were highlighted in the plot (and vice versa). For all samples analysed, the spatial location of (i) outliers highlighted by the robust regression approach and (ii) visually aligned high $^{238}U/^{206}Pb$ ratio points in the TW plot were identified. In either case (or both), if the identified pixels are located in close spatial proximity on the map, a subset of the map can be selected and the age calculated from the pixels in that subset. It should be noted, however, that due to the small number of pixels selected, the age obtained is not necessarily more accurate than using the entire map (as also highlighted by Drost et al. (2018) regarding their approach).

3 Results

For all samples considered in this study, the three types of diagrams used for age calculations (TW, 86TW and isochron) are presented in the Supplementary material.

https://doi.org/10.5194/gchron-2020-10
This is just a preview and not the published preprint.
© Author(s) 2020. CC-BY 4.0 License.

3.1. Age determination on previously dated samples

3.1.1. Duff Brown

The ages were obtained by regression in the TW space on 2 images chosen as an example. The ages found without anchoring the common lead value are 54.7 ± 3.8 Ma (Fig. 2B, 2C) and 57.8 ± 3.2 Ma (not shown), younger than the reference value of 64.04 ± 0.7 Ma (Hill et al., 2016). This is due to Pb_0 values lower than that calculated from data of Hill et al. (2016) (0.738 ± 0.01, 1s). The discrepancy between both values is explained by the high $^{238}U/^{206}Pb$ ratio of the sample (typically 60-70) that prevents a precise determination of the common lead value. Using the reference Pb_0 value leads to ages of 63.1 ± 2.2 Ma (Fig. 2D, 2E) and 64.7 ± 2.3 Ma (not shown), similar to the reference value within uncertainties. Note that the maps used for age calculation (Fig. 2A) are smaller (0.21 mm^2, ~630 pixels) than those made for other samples as Duff Brown was used as a secondary standard during the tests, which explains the rather large age uncertainty. The high d-MSWD values are in this case due to the low $^{207}Pb/^{206}Pb$ values of the pixels the closest to the y-axis (i.e., with lower $^{238}U/^{206}Pb$ value) compared to those expected from the anchored regression.

3.1.2. BH14

This sample has a large variation in the U/Pb ratios and a large amount of U, which allows precise dating as shown by Beaudoin et al. (2018). Two images taken at two distinct locations in the same vein clearly show this variation in isotope ratios and U concentrations, which appears to be related to crystal growth zoning (Fig. 3A, 3B). The ages obtained from the entire maps vary between 60.7 ± 2 Ma and 61.8 ± 2.5 Ma according to the diagrams considered (Fig. 3C, 3D; only TW concordia plots shown). They are identical within the limits of uncertainty to that obtained by Beaudoin et al. (2018) (63.2 ± 2.2 Ma) and to that obtained by LA-ICPMS spot analysis in our laboratory (61.2 ± 2.9 Ma; Fig. 3G). The uncertainties on the age before propagation of uncertainties are generally less than 1 Ma, similar to that obtained by spot analysis. This high precision can be related to the very good visual and statistical parameters calculated for this regression (good point alignment, very low RSE, and low d-MSWD (Fig. 3C, 3D, 3E, 3F)). The colocalization study shows that the points furthest from the trend line of the robust regression are not located in a same area on the isotopic map. Any selection of a part of the map to possibly improve the age calculations is not justified.

3.1.3. PXG20-1

The age values obtained by robust regression on the PXG20-1 sample are comparable within the uncertainties between the TW concordia plot (Fig. 4B, 4D), the 86TW plot (Fig. 4C) and the isochron plot (Fig. S3). They are consistent with the very robust age obtained by LA-ICPMS spot analysis (40.5 ± 2.3 Ma), both in terms of absolute value and precision (Fig. 4E). However, there are slight variations in the central age depending on the diagram used, with ages of about 40.5 ± 2 Ma for the TW and isochron diagrams, but 38.3 ± 2.1 Ma for the TW86 diagram. These differences can be related to the statistical parameters of the regression which are not as good as those obtained for BH14 or for the LA-ICPMS spot analysis. This

https://doi.org/10.5194/gchron-2020-10
This is just a preview and not the published preprint.
© Author(s) 2020. CC-BY 4.0 License.

possibly shows some heterogeneity of isotopic composition, such as for example inclusions of detrital material. The colocalization study shows a globally homogeneous spatial distribution of the values most distant from the regression line in a TW concordia plot. Any inclusions or cement alteration would certainly be better highlighted using a thresholding approach as proposed by Drost et al. (2018). Finally, the ages obtained with both the isotope mapping approach and LA-ICPMS spot analysis are centered around 40 Ma, with the exception of the TW86 regression. Such ages are similar to that suggested by the paleomagnetic study of Oms et al. (2003), which point to a Bartonian age (~40-38.5 Ma). However, they are slightly older (including within the limits of uncertainty) than the age proposed by Canudo and Molina (1988) on the basis of the presence of *Globigerinatheka semi-involuta* in the sediments containing the sample. This microfauna rather indicates an age between 38.5 and 36 Ma according to Premoli-Silva et al. (2006) and Wade et al. (2011), and considering the GTS2012 (Gradstein et al., 2012). The origin of this discrepancy is not yet identified. Nevertheless, the ages obtained are consistent, along with the other proxies, with the transition between marine and continental deposits in the studied area being Bartonian-Priabonian in age.

3.1.4. PXG32-2

The values obtained for this lake carbonate sample are identical for all the regressions, with a value of ~35 ± 2 Ma (Fig. 5B, 5C; only the TW concordia plot is shown). All these ages are similar within the limits of uncertainty and in agreement with the one obtained by LA-ICPMS spot analysis (37 ± 3 Ma; Figure 5D), and by the paleomagnetic study of Mochales et al. (2016). The age obtained with the robust regression approach is of higher precision than the age found with LA-ICPMS spot analysis. However, the age calculated with spot analysis is associated with unsatisfactory statistics (MSWD = 6.3) and could therefore be considered as an errorchron. Such high MSWD is clearly linked with sample heterogeneity as seen from the scatter of error ellipses around the regression line (Fig. 5D). Compositional heterogeneities are also clearly visible with U and Pb elemental maps (Fig. 5A). This is consistent with the heterogenous nature of the sample, composed of pellets and microbial oncoids (Fig. S2). The colocalization study indicates that there are no obvious links between such heterogeneities and the location of outlier pixel values, which are evenly distributed on the maps and do not justify any sub-selection of the isotopic map. The statistical parameters of the regressions calculated with the mapping approach also appear to be very good. The age obtained confirms the Bartonian age of the first continental deposits in the eastern part of the Jaca Basin in the southern Pyrenees, bringing an absolute constraint on the end of non-deposition period above the Boltana anticline.

3.2. Unknown samples

3.2.1. ETC2

The isotopic map of this sample (Fig. 6A), taken from a tectonic breccia in the Basque Country (France), was made through several calcite cements as clearly shown in the cathodoluminescence images (Fig. 6C). An age obtained from all the pixels can therefore potentially correspond in reality to a mixture of ages and distinct values of common lead. When taking the entire

https://doi.org/10.5194/gchron-2020-10
This is just a preview and not the published preprint.
© Author(s) 2020. CC-BY 4.0 License.

map to calculate an age, some dispersion in the $^{207}Pb/^{206}Pb$ values for the weakly radiogenic pixels can be noticed (Fig. 6B). Nevertheless, the ages obtained are identical within the limits of uncertainty: 97.0 ± 4.6 Ma and 97.0 ± 4.8 for the TW (Fig. 6B) and 86TW plots (not shown), respectively, and an age of 95.9 ± 3.5 Ma for the isochron plot (not shown). These similar ages are consistent with the good statistical parameters obtained from the robust regression. However, both the maps of pixel concentration values and the colocalization analysis of image data demonstrate that the overdispersion of $^{207}Pb/^{206}Pb$ values are located in a restricted area of the map corresponding to one cement (cement C1 on the CL image, Fig. 6C), whereas the highest $^{238}U/^{206}Pb$ (i.e., most radiogenic values) that drive the age are located in another restricted area corresponding to another cement (cement C2 on the CL image) (Fig. 6D). Lead by the colocalization study, the selection of a small area of the map corresponding to cement C2 results in similar but more accurate age calculations than considering the entire map (97.6 ± 4.2 Ma for the TW plot (Fig. 6E), 97.1 ± 4.1 Ma for the 86TW (Fig. S3) and 95.4 ± 3.4 Ma for the isochron plot (Fig. S3)). The statistical parameters are also better, despite a number of pixels divided by three. This demonstrates the relevance of the colocalization approach for isotope maps, especially when the analytical conditions do not allow trace elements to be analyzed at the same time as U and Pb.

Finally, the age obtained indicates cement precipitation during the rifting event that affected the area before the Iberian-Eurasian convergence that led to the formation of the Pyrenees from the Campanian (Mouthereau et al., 2014).

3.2.2. ARB

ARB sample is a single, homogenous calcite cement partially filling a tectonic breccia. The calculated ages for this sample are 106.6 ± 4.4 Ma for the TW concordia plot, 107.5 ± 4.2 Ma for the 86TW plot and 109.7 ± 3.6 Ma for the isochron if the entire image is considered (not shown). Again, these values are similar within uncertainties. The slight age differences between the types of plots (< 3%) may be related to the high d-MSWD (greater than 2 for the TW regression), in line with a moving average showing deviations from the regression line. The colocalization study indicates that among the more distant points from the regression line in the concordia TW plot almost all correspond to pixels located in the left quarter of the isotope map (Fig. 7A). The uncertainties on age obtained without considering these pixels are similar to those obtained with the whole map: 107.1 ± 4.4 Ma for the TW concordia plot (Fig. 7B), 108.0 ± 4.2 Ma for the 86TW plot (Fig. S3) and 109.7 ± 3.6 Ma for the isochron (Fig. S3). However, contrary to ETC2, the statistical parameters are worse due to the disappearance of several pixels located close to the robust regression line.

Taken together, ETC2 and ARB samples suggest that the emplacement of tectonic breccia in the western Pyrenees was related to extensive syn-rift fault development, rather than to the subsequent tectonic inversion.

https://doi.org/10.5194/gchron-2020-10
This is just a preview and not the published preprint.
© Author(s) 2020. CC-BY 4.0 License.

5 Discussion

5.1. Interest of dating from isotope maps

The pioneering work of Drost et al. (2018) has shown the obvious value of the isotope map dating approach, where data on minor and trace element concentrations are used to select the most suitable pixels for age determination. This initial step seems really essential and should be followed up systematically if the analytical conditions makes it possible (e.g. use of an ICPMS with a fast mass scan such as a quadrupole or TOF). If not, the operator must remain attentive to the quality of the data, by checking the scattering of the pixels around the regression lines and the possible presence of phase mixtures. The use of a colocalization approach as presented in our study is an efficient way to carry out this careful study of the spatial distribution of the furthest pixel values from the regression line. It is in any case fundamental to carry out an initial petrographic characterization of the samples as recalled by Roberts et al. (2019). Taking these precautions into account, our results and those of Drost et al. (2018) and Roberts et al. (2019) show that the ages obtained from the image mapping approach are perfectly comparable, both in value and uncertainty, with those obtained from more common methods (LA-ICPMS spot analysis and isotope dilution). Additionally, it should be pointed out that this approach has several advantages in comparison with the more common ones. First, the image mapping approach is particularly suitable for easily dating multiple generations of cements filling porosities or fractures. Such an approach is fast and simple to set up, since it is sufficient to map a large portion of the sample under consideration to cover several generations of cements with number of pixels high enough for age calculation, and then to select the pixels (by a geochemical and/or colocalization approach) corresponding to the different cements to calculate the ages. This methodology has been carried out successfully on sample ARB. Second, the LA-ICPMS maps can be built directly on thin sections (work of Drost et al., 2018) or on thick sections (this work), allowing ideally to gather on a same section all petrographic and geochemical work necessary to give trustful ages on a single sample, which may save a considerable amount of time. It is therefore likely that this method to U-Pb dating of carbonates will develop rapidly in the geochronology community, alongside with the now well-established LA-ICPMS spot analysis approach.

5.2. Benefits and limitations of the robust regression to U-Pb image dating

The data processing method presented here, namely the robust regression through the isotope ratio values of the pixels represented in TW or isochron diagrams, is simple and allows a fast age determination and its uncertainty. As an alternative to the data pooling approach presented by Drost et al. (2018), it has the advantage of not involving the operator in the choice of the number of pixels in each ‘pseudoanalysis’, since all pixels are considered for a single regression. Their representation in the appropriate diagrams gives a quick idea of the quality of the data, assisted by statistical parameters such as RSE or d-MSWD. Note that the interest of using robust regression for U-Pb dating was already underlined by Powell et al. (2002) and very recently by Powell et al. (2020). It is also implemented in the famous Isoplot software (Ludwig, 2012). Ludwig (2012) stressed the precautions to be taken when using robust regression to construct isochrons, since the absence of uncertainties on each point makes it impossible to distinguish the share of scatter around the regression due to "geological/geochemical

https://doi.org/10.5194/gchron-2020-10
This is just a preview and not the published preprint.
© Author(s) 2020. CC-BY 4.0 License.

complications" from that due to analytical errors alone. In conventional spot analyses, the MSWD calculation is an efficient way to determine the share of each source of uncertainty. Its use in the context of dating from isotopic images, whether with the approach of Drost et al. (2018) or our own, does not solve this problem since the MSWD is calculated from an "artificial" grouping of pixels whose associated ellipses do not represent analytical uncertainties. At most, the MSWD (or d-MSWD) is here a means of verifying the correct alignment of values in the TW and isochron diagrams, with values close to 1 indicating good alignment, information that can be complemented by the moving average calculation as we propose, among other possibilities. For example, the very recent approach proposed by Powell et al. (2020), with calculation of a normalized (robust) median of the absolute values of the residuals, could provide a suitable means to distinguish isochrons from errorchrons. It still has to be implemented in our data reduction scheme.

6 Conclusion

U-Pb LA-ICPMS carbonate dating from isotope images is an extremely recent approach which, compared to more common dating methods such as LA-ICPMS spot analyses, has the great advantage of allowing the use of images for both sample screening and dating. In this contribution, U-Pb ages of several carbonate samples were obtained from micro-scale LA-ICPMS isotopic maps, using a new, alternative data processing method based on robust regression. The method, which is very simple to set up, consists of extracting the U/Pb and Pb/Pb pixel values from the image, plotting them in a diagram used for dating such as a concordia diagram, and performing robust regression to calculate the age. Prior to dating, we also conducted a colocalization study of the sample isotope ratios that was used to locate the most suitable areas to age determination. For samples that had already been dated by U-Pb geochronology using conventional LA-ICPMS spot analysis or isotope dilution, the robust regression approach method provided similar ages and sometimes better uncertainties compared to both others methods, with an ablation duration less than 40 min. The robust regression processing of LA-ICPMS isotope map data thus appears to be a simple and efficient means to proceed to carbonate U-Pb geochronology.

7 Appendix

7.1 Analytical conditions

Laboratory & Sample Preparation	
Laboratory name	Institut des sciences analytiques et de physico-chimie pour l'environnement et les matériaux (IPREM), UPPA, Pau (France)
Sample type/mineral	Calcite
Sample preparation	In situ in polished blocks
Imaging	Two per sample (one for sample screening and one for dating)
Laser ablation system	
Make, Model & type	Lambda 3, Nexeya (France)

https://doi.org/10.5194/gchron-2020-10
This is just a preview and not the published preprint.
© Author(s) 2020. CC-BY 4.0 License.

Laser wavelength (nm)	257 nm	
Pulse duration (fs)	360 fs	
Fluence ($J.cm^{-2}$)	5-8 $J.cm^{-2}$	
	Preliminary imaging	***Isotope dating maps***
Repetition rate (Hz)	300 Hz	500 Hz
Gas blank (s)	No	42 s to 74 s per image (1 line)
Ablation duration (s)		19 min to 38 min
Washout and/or travel time in between analyses (s)	Wash out time: 500 ms (He) or 1000 ms (Ar). 15 s of break between lines to allow data processing	
Spot diameter (µm)	17 µm	
Sampling mode / pattern	Ablation lines (50 µm-width) made by combining laser beam movement across the surface (10 mm/s) and stage movement (100 µm/s). 100 µm between lines.	Ablation lines (25 µm-width) made by combining laser beam movement across the surface (5 mm/s) and stage movement (25 µm/s). 25 µm between lines.
Cell Carrier gas (L/min)	Ar = 0.650-0.700 L/min (october 2018) or He = 0.600 L/min (April 2019, October 2019)	
ICP-MS Instrument		
Make, Model & type	ICPMS Thermo Fisher Element2 HR Jet Interface	
RF power (W)	1000 - 1100W	
Cooling gas flow rate	16 L min^{-1}	
Auxiliary gas flow rate	1 L min^{-1}	
Nebuliser gas flow rate	0.5 L min^{-1}	
Masses measured	206,207,238	206, 207, 208, 232, 238
Samples per peak	40	30
Mass window	50 %	10 %
Sample time	8.3 ms	3 ms
Settling time	1 ms	1 ms
Mass sweep	500 ms	60 ms
Averaged mass sweep	2	8
Resolution	300	
Data Processing		
Calibration strategy	No	Calibration by standard bracketing; NIST614 (October 2018) and 612 (April, October 2019) for Pb-Pb and WC-1 calcite for Pb-U
Reference Material info	No	Primary: NIST614 / 612 - Woodhead and Hergt (2001) WC-1 254 ± 6 Ma (2s) - Roberts et al., 2017 Secondary: Duff Brown 64.04 +/- 0.67 Ma (2s) - Hill et al., 2016
Data processing package used / Correction for LIEF	Element XR acquisition software, data processing with in-house Python code and ImageJ software.	

© Author(s) 2020. CC-BY 4.0 License.

Common-Pb correction, composition and uncertainty	No	No common Pb correction. Unanchored robust regressions in Tera-Wasserburg, 86TW plot (Parrish et al., 2018) and $^{206}Pb/^{208}Pb_{common}$ versus $^{238}U/^{208}Pb_{common}$ isochron plots. Ages in the data table are quoted at 95% absolute uncertainties and include systematic uncertainties, propagation is by quadratic addition.
Quality control / Validation	No	4 analyses of Duff Brown (anchored to common Pb value of 0.738) gave ages of 66.87 ± 2.48 Ma (April 2019), 67.79 ± 2.38 Ma, 65.76 ± 2.30 Ma, 64.67 ± 2.29 Ma and 63.06 ± 2.17 Ma (October 2019)

8 Author contribution

GH, FC, CP designed the experiments. GH, FC, CP, PAG, GM carried them out. GH and CP developed the model code and performed the simulations. OC and JPG supervised the project and provided the financial support for most experiments. GH prepared the manuscript with contribution from all co-authors.

9 Competing interests

The authors declare that they have no conflict of interest.

10 Acknowledgements

Gaëlle Barbotin is thanked for help during the analytical sessions. This work benefited from funding from the Université de Pau et Pays de l'Adour (AAP Incitatif Recherche) and from Total (project DAC).

11 References

Aramendía, M., Rello, L., Bérail, S., Donard, A., Pécheyran, C., and Resano, M.: Direct analysis of dried blood spots by femtosecond-laser ablation-inductively coupled plasma-mass spectrometry. Feasibility of split-flow laser ablation for simultaneous trace element and isotopic analysis. *Journal of Analytical Atomic Spectrometry, 30(1)*, 296-309, 2015

Ballihaut, G., Claverie, F., Pécheyran, C., Mounicou, S., Grimaud, R. and Lobinski, R.: Sensitive Detection of Selenoproteins in Gel Electrophoresis by High Repetition Rate Femtosecond Laser Ablation-Inductively Coupled Plasma Mass Spectrometry. *Analytical Chemistry, 79*, 6874-6880, 2007

Beaudoin, N., Lacombe, O., Roberts, N.M.W. and Koehn, D.: U-Pb dating of calcite veins reveals complex stress evolution and thrust sequence in the Bighorn Basin, Wyoming, USA. *Geology, 46 (11)*, 1015-1018, doi: 10.1130/G45379.1, 2018.

© Author(s) 2020. CC-BY 4.0 License.

Canudo J.I. and Molina E.: Biocronología de foraminíferos planctónicos de la secuencia deposicional de Jaca (Pirineo Aragonés): Eoceno medio y superior. I*n: II Congreso Geológico de España, Granada. Comunicaciones, 1*, 273−276 (in Spanish), 1988.

Drost, K., Chew, D., Petrus, J. A., Scholze, F., Woodhead, J. D., Schneider, J. W. and Harper, D. A. T: An image mapping approach to U-Pb LA-ICP-MS carbonate dating and applications to direct dating of carbonate sedimentation. *Geochemistry, Geophysics, Geosystems, 19*, 46314648. https://doi.org/10.1029/2018GC007850, 2018.

Godeau N., Deschamps P., Guihou A., Leonide P., Tendil A., Gerdes A., Hamelin B. and Girard J.-P.: U-Pb dating of calcite cement and diagenetic history in microporous carbonate reservoirs: Case of the Urgonian Limestone, France. *Geology*, https://doi.org/10.1130/G39905.1, 2018

Gradstein, F.M., Ogg, J.G., Schmitz, M.D. and Ogg, G.M., (coordinators), et al.: The Geologic Time Scale 2012. *Elsevier, Boston, USA*. 1174 p. (2-volume book), 2012.

Hill, C. A., Polyak, V. J., Asmerom, Y. and Provencio, P.P.: Constraints on a Late Cretaceous uplift, denudation, and incision of the Grand Canyon region, southwestern Colorado Plateau, USA, from U-Pb dating of lacustrine limestone, *Tectonics, 35*, 896–906, doi:10.1002/2016TC004166, 2016

Horstwood, MSA, Košler, J, Gehrels, G, Jackson, SE, Mclean, NM, Paton, C, Pearson, NJ, Sircombe, K, Sylvester, P, Vermeesch, P, Bowring, JF, Condon, DJ and Schoene, B.: CommunityDerived Standards for LA-ICP-MS U-(Th-)Pb Geochronology - Uncertainty Propagation, Age Interpretation and Data Reporting. *Geostandards and Geoanalytical Research, 40(3)*, 311332, doi :10.1111/j.1751-908X.2016.00379.x, 2016

Koller, M. and Stahel, W.A.: Sharpening Wald-type inference in robust regression for small samples. *Computational Statistics & Data Analysis, 55(8)*, 2504-2515, 2011

Koller, M. and Stahel, W.A.: Nonsingular subsampling for regression S~estimators with categorical predictors, *Computational Statistics, 32(2),* 631-646. 10.1007/s00180-016-0679-x, 2017

Li, Q., Parrish, R.R., Horstwood, M.S.A. and McArthur, J.M.: U–Pb dating of cements in Mesozoic ammonites. *Chemical Geology, 376*, 76-83, 2014.

Ludwig, K. R. User's manual for Isoplot version 3.75–4.15: a geochronological toolkit for Microsoft Excel. *Berkeley Geochronological Center Special Publication, 5*, 2012.

Maechler, M., Rousseeuw, P., Croux, C., Todorov, V., Ruckstuhl, A., Salibian-Barrera, M., Verbeke, T., Koller, Conceicao, E.L.T. and Anna di Palma, M.: robustbase: Basic Robust Statistics R package version 0.93-5. http://CRAN.R-project.org/package=robustbase, 2019

Mochales, T., Pueyo, E.L., Casas, A.M. and Barnolas, A.: Restoring paleomagnetic data in complex superposed folding settings: the Boltaña anticline (Southern Pyrenees). *Tectonophysics, 671*, 281-298, 2016

Mouthereau, F., Filleaudeau, P.Y., Vacherat, A., Pik, R., Lacombe, O., Fellin, M.G., Castelltort, S., Christophoul, F. and Masini, E.: Placing limits to shortening evolution in the Pyrenees: role of margin architecture and implications for the Iberia/Europe convergence. *Tectonics*. http://dx.doi.org/10.1002/2014TC003663, 2014

© Author(s) 2020. CC-BY 4.0 License.

Nuriel, P., Craddock, J., Kylander-Clark, A.R., Uysal, T., Karabacak, V., Dirik, R.K., Hacker, B.R. and Weinberger, R.: Reactivation history of the North Anatolian fault zone based on calcite age-strain analyses. *Geology, 47*, 465-469, 2019.

Oms, O., Dinarès-Turell, J. and Remacha, E.: Magnetic stratigraphy from deep clastic turbidites: An example from the Eocene Hecho Group (southern Pyrenees). *Studia Geophysica et Geodetica, 47(2)*, 275-288, 2013.

Parrish, R.R., Parrish, C.M. and Lasalle, S.: Vein calcite dating reveals Pyrenean orogen as cause of Paleogene deformation in southern England. Journal of the Geological Society, https://doi.org/10.1144/jgs2017-107, 2018.

Poitrasson, F. and d'Abzac, F.-X.: Femtosecond laser ablation inductively coupled plasma source mass spectrometry for elemental and isotopic analysis: are ultrafast lasers worthwhile? Journal of Analytical Atomic Spectrometry, 32, 1075-1091, 2017.

Powell, R., Woodhead, J, and Hergt, J.: Improving isochron calculations with robust statistics and the bootstrap. *Chemical Geology 185*, 91–204, 2002.

Powell, R., Green, E. C. R., Marillo Sialer, E., and Woodhead, J.: Robust Isochron Calculation, *Geochronology Discuss.*, https://doi.org/10.5194/gchron-2020-4, in review, 2020.

Premoli Silva, I., Wade, B. S. and Pearson, P. N.: Taxonomy, biostratigraphy, and phylogeny of Globigerinatheka and Orbulinoides. In, Pearson, P. N. , Olsson, R. K. , Hemleben, C. , Huber, B. T. and Berggren, W. A. (eds) *Atlas of Eocene Planktonic Foraminifera.* Cushman Foundation for Foraminiferal Research, Special Publication. 41(Chap 7), 169-212, 2016.

Roberts, N. M. W., Drost, K., Horstwood, M. S. A., Condon, D. J., Chew, D., Drake, H., Milodowski, A. E., McLean, N. M., Smye, A. J., Walker, R. J., Haslam, R., Hodson, K., Imber, J. and Beaudoin, N.: LA-ICP-MS U-Pb carbonate geochronology: strategies, progress, and application to fracture-fill calcite, *Geochronology Discuss.*, https://doi.org/10.5194/gchron-2019-15, in review, 2019.

Roberts, N. M. W., Rasbury, E. T., Parrish, R. R., Smith, C. J., Horstwood, M. S. A. and Condon, D. J.: A calcite reference material for LA-ICP-MS U-Pb geochronology: *Geochemistry, Geophysics, Geosystems,* doi:10.1002/2016GC006784, 2017

Roberts, N.M.W. and Walker, R.J.: U-Pb geochronology of calcite-mineralized faults: Absolute timing of rift-related fault events on the northeast Atlantic margin. *Geology, 44*, 531-534, 2016.

Vermeesch, P.: IsoplotR: A free and open toolbox for geochronology. *Geoscience Frontiers, 9*, 1479-1493, doi: 10.1016/j.gsf.2018.04.001, 2018

Wade, B.S., Pearson, P.N., Berggren, W.A. and Pälike, H.: Review and revision of Cenozoic tropical planktonic foraminiferal biostratigraphy and calibration to the geomagnetic polarity and astronomical time scale. *Earth-Science Reviews, 104*, 111–142, 2011.

Woodhead, J. D. and Hergt, J. M.: Strontium, neodymium and lead isotope analyses of NIST glass certified reference materials: SRM 610, 612, 614. *Geostandards Newsletter, 25(2–3)*, 261–266, doi: 10.1111/j.1751-908X.2001.tb00601.x, 2001.

Zeitvogel, F. and Obst, M. ScatterJn: An ImageJ Plugin for Scatterplot-Matrix Analysis and Classification of Spatially Resolved Analytical Microscopy Data. *Journal of Open Research Software, 4(1)*, p.e5. DOI: http://doi.org/10.5334/jors.89, 2016.

https://doi.org/10.5194/gchron-2020-10
This is just a preview and not the published preprint.
© Author(s) 2020. CC-BY 4.0 License.

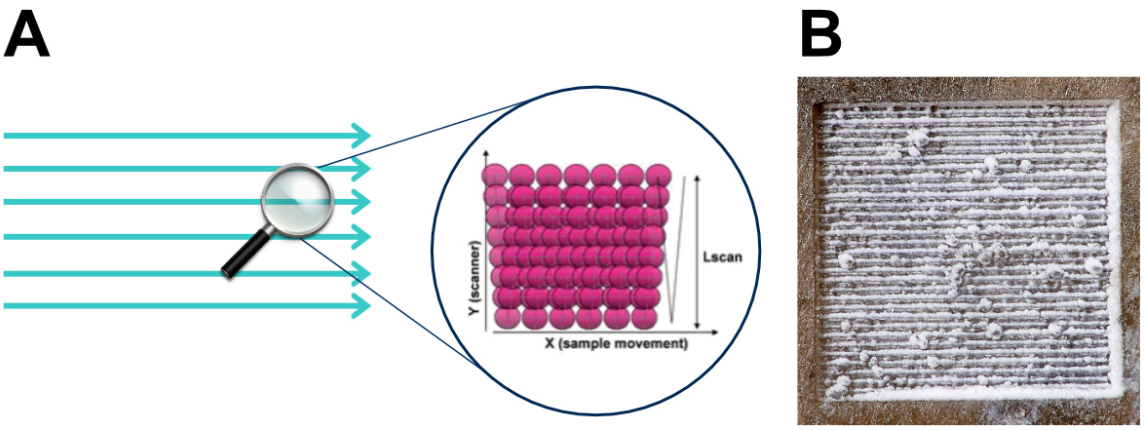

Figure 1: A: Principle of the construction of the ablation lines with the femtosecond laser used in the study. Lscan corresponds to the width of the line, here 50 µm or 25 µm. B: Example of ablation produced by the rasters used for producing an isotopic map (dimensions: 800 µm x 800 µm).

https://doi.org/10.5194/gchron-2020-10
This is just a preview and not the published preprint.
© Author(s) 2020. CC-BY 4.0 License.

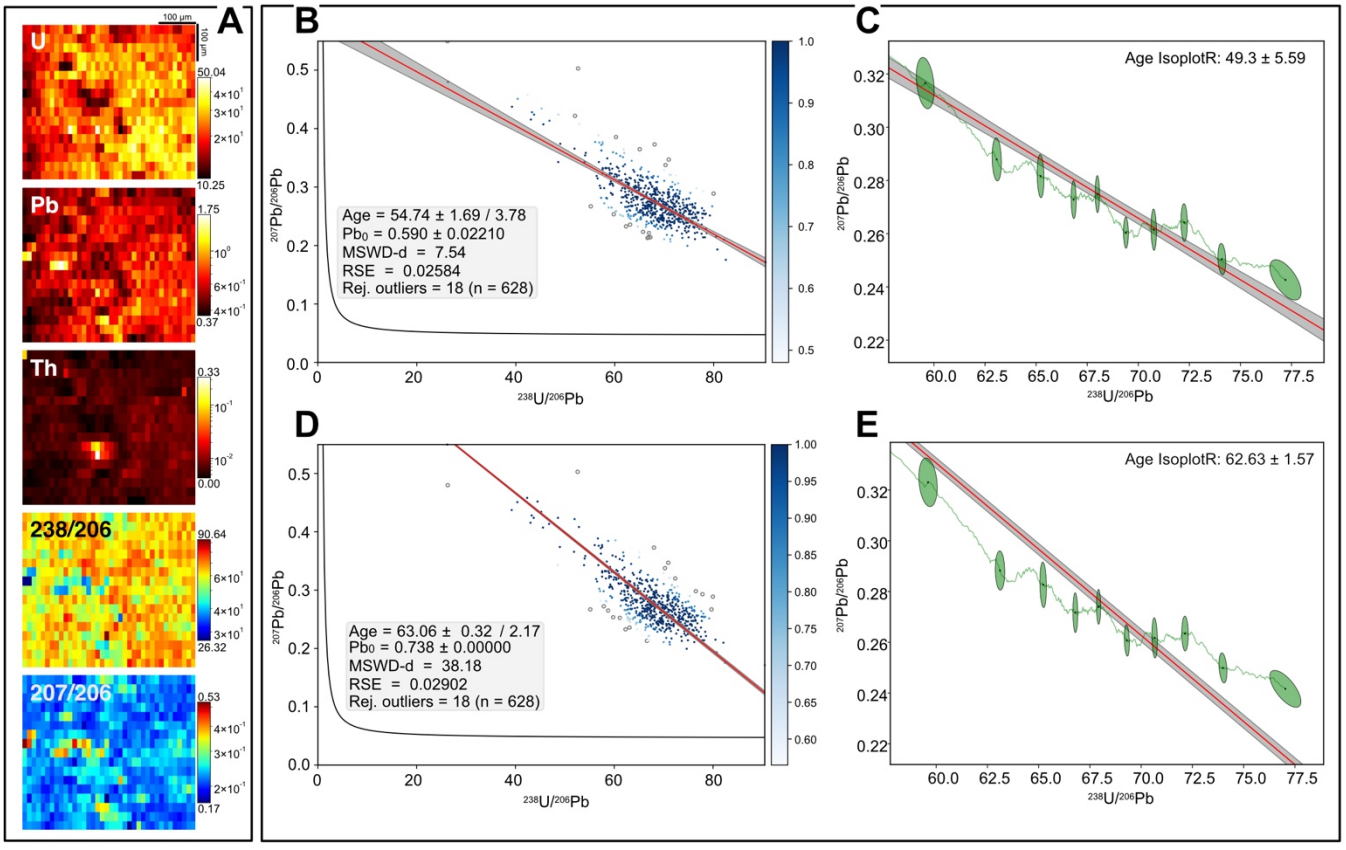

Figure 2: A: Element concentrations in ppm (U, Pb, Th) and $^{238}U/^{206}Pb$, $^{207}Pb/^{206}Pb$ isotopic maps obtained for one analysis of Duff Brown sample. Note that the concentrations are normalized to the mean number of counts measured in the NIST standard for the considered masses, and should thus be regarded only as semi-quantitative. B: TW concordia plots with age calculated by robust regression, without anchoring the common Pb value. The age uncertainties (1.96σ level) are without (left) and with uncertainty propagation (right). C: TW concordia plot with pseudo-ellipses corresponding to the sets obtained by the discretization of the pixel ratio values used for regression, and used for calculation of the d-MSWD (see text for details). The regression and associated confidence interval are those obtained by the robust regression. The age obtained by York-type regression using IsoplotR on the same sets is also indicated, along with studentized age uncertainty taking account the overdispersion for MSWD values > 1 (see Vermeesch, 2018 for details). D: Same as A but with common Pb anchored to a value of 0.738 as calculated from Hill et al. (2016). E: Same as C for the anchored robust regression.

https://doi.org/10.5194/gchron-2020-10
This is just a preview and not the published preprint.
© Author(s) 2020. CC-BY 4.0 License.

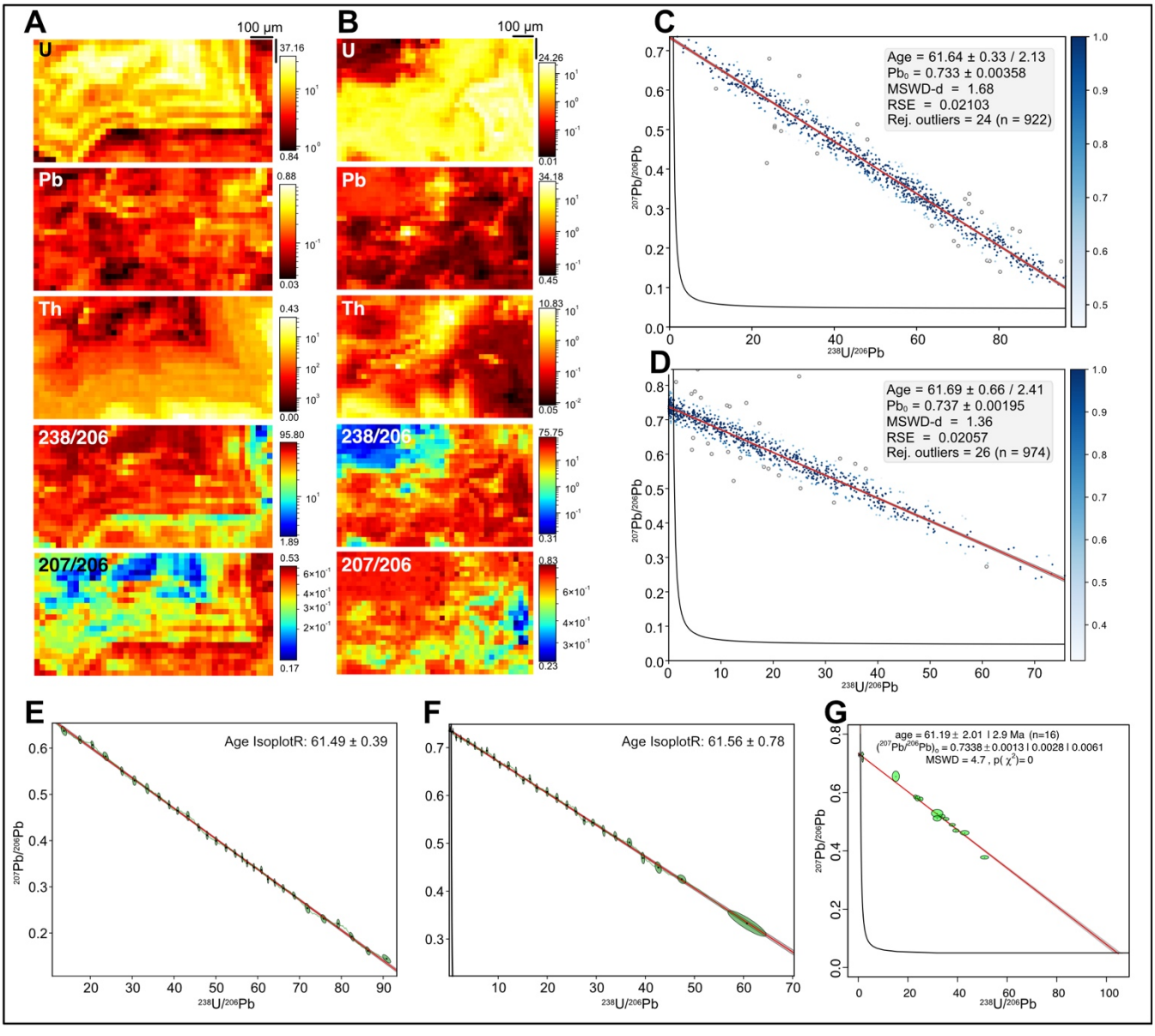

Figure 3: Results obtained for two isotopic maps of sample BH14 (A, C, E: first map; B, D, F: second map). A, B: Semi-quantitative element concentrations in ppm (U, Pb, Th) and $^{238}U/^{206}Pb$, $^{207}Pb/^{206}Pb$ isotopic maps. C, D: TW concordia plots with ages and their uncertainty calculated by robust regression. E, F: TW concordia plots with pseudo-ellipses used for calculation of the d-MSWD, with age and associated uncertainty (without systematic uncertainties) obtained by York-type regression using IsoplotR also indicated. G: TW concordia plot obtained from LA-ICPMS spot analyses. Ages and associated uncertainties were obtained from York-type regression using IsoplotR (age uncertainties (1.96σ level) are without (left) and with systematic uncertainty (right)).

https://doi.org/10.5194/gchron-2020-10
This is just a preview and not the published preprint.
© Author(s) 2020. CC-BY 4.0 License.

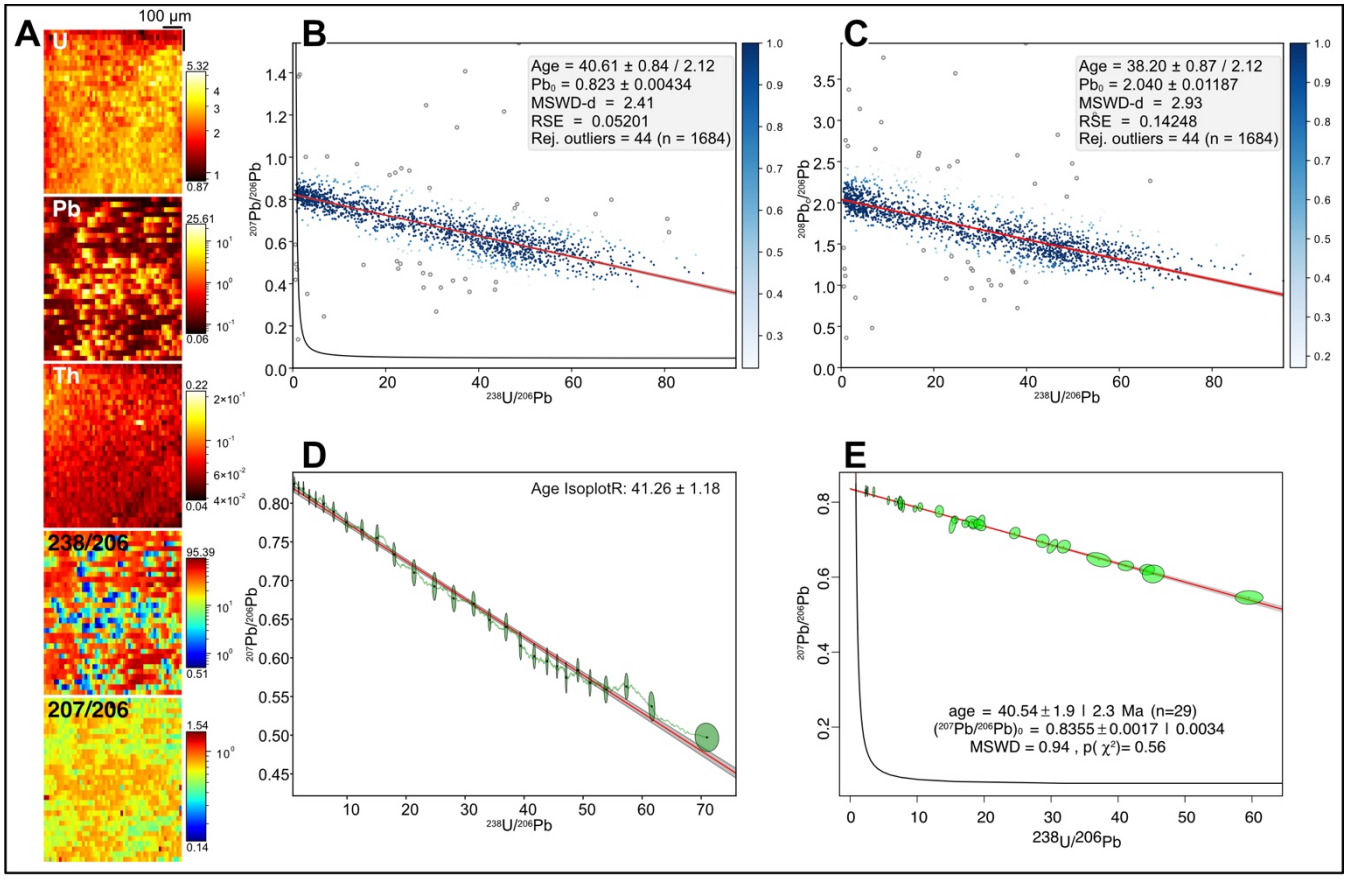

Figure 4: Results obtained for sample PXG20-1. A: Semi-quantitative element concentrations in ppm (U, Pb, Th) and $^{238}U/^{206}Pb$, $^{207}Pb/^{206}Pb$ isotopic maps. B, C: TW and 86TW plots with ages and their uncertainty calculated by robust regression. D: TW concordia plot with pseudo-ellipses used for calculation of the d-MSWD. Age and associated uncertainty obtained by York-type regression using IsoplotR are also indicated. E: TW concordia plot obtained from LA-ICPMS spot analyses. Ages and associated uncertainties were obtained from York-type regression using IsoplotR.

https://doi.org/10.5194/gchron-2020-10
This is just a preview and not the published preprint.
© Author(s) 2020. CC-BY 4.0 License.

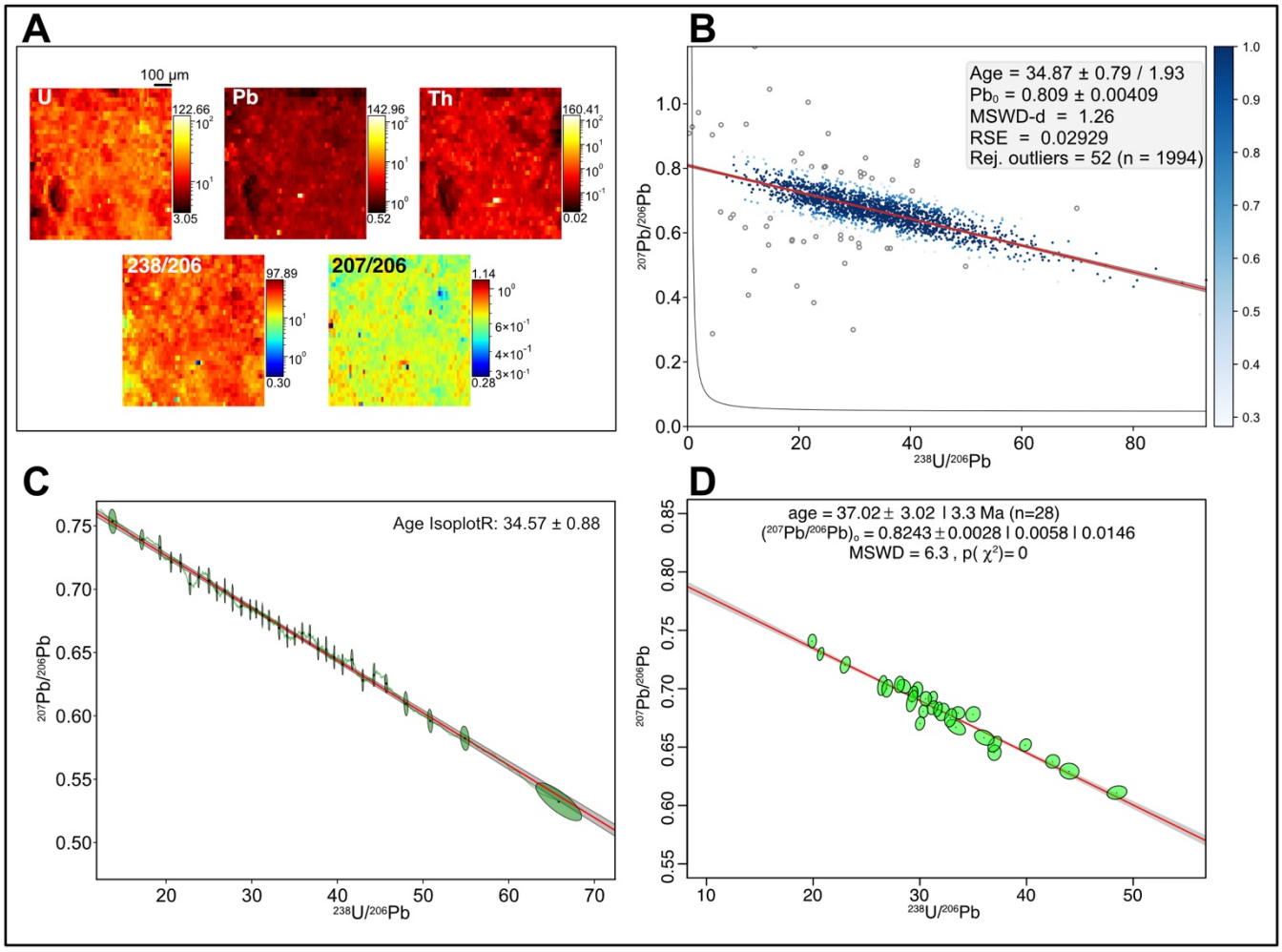

Figure 5: Results obtained for sample PGX32-2. A: Semi-quantitative element concentrations in ppm (U, Pb, Th) and $^{238}U/^{206}Pb$, $^{207}Pb/^{206}Pb$ isotopic maps. B: TW concordia plot with ages and their uncertainty calculated by robust regression. C: TW concordia plot with pseudo-ellipses used for calculation of the d-MSWD. Age and associated uncertainty obtained by York-type regression using IsoplotR are also indicated. D: TW concordia plot obtained from in situ LA-ICPMS analyses. Ages and associated uncertainties were obtained from York-type regression using IsoplotR.

https://doi.org/10.5194/gchron-2020-10
This is just a preview and not the published preprint.
© Author(s) 2020. CC-BY 4.0 License.

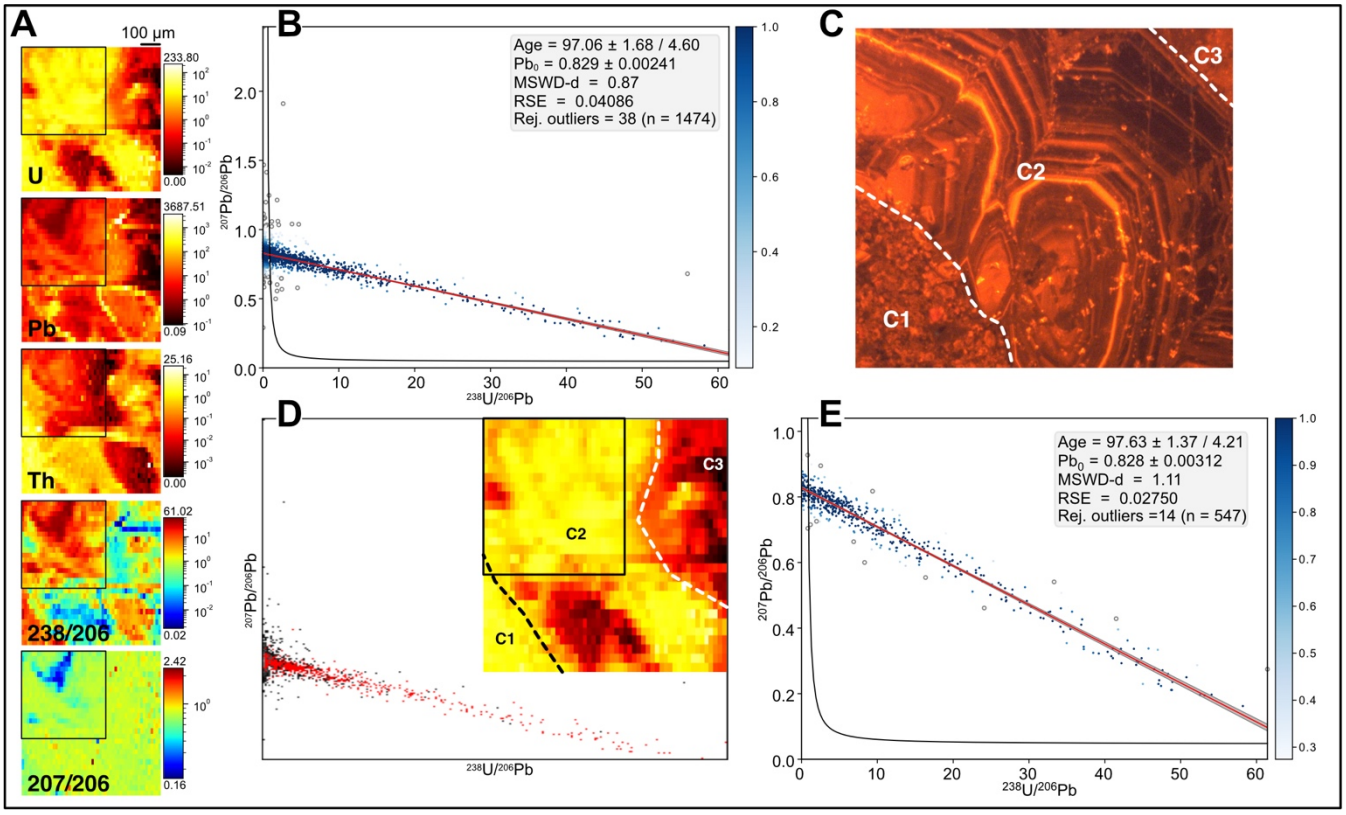

Figure 6: Results obtained for sample ETC2. A: Semi-quantitative element concentrations in ppm (U, Pb, Th) and $^{238}U/^{206}Pb$, $^{207}Pb/^{206}Pb$ isotopic maps. Black frames correspond to the image subset selected by colocalization. B: TW concordia plot with ages and their uncertainty calculated by robust regression for the entire map. C: Cathodoluminescence image of an area close to that of the image map. Three distinct cements are distinguished (C1 to C3). D: $^{207}Pb/^{206}Pb$ versus $^{238}U/^{206}Pb$ scatterplot obtained with the ScatterJn plugin from the isotopic maps. Red dots correspond to the pixels of the image subset (black frame in A and on the Uranium concentration map where the approximate location of distinct cement is given). D: TW concordia plot with ages and their uncertainty calculated by robust regression for the image subset.

https://doi.org/10.5194/gchron-2020-10
This is just a preview and not the published preprint.
© Author(s) 2020. CC-BY 4.0 License.

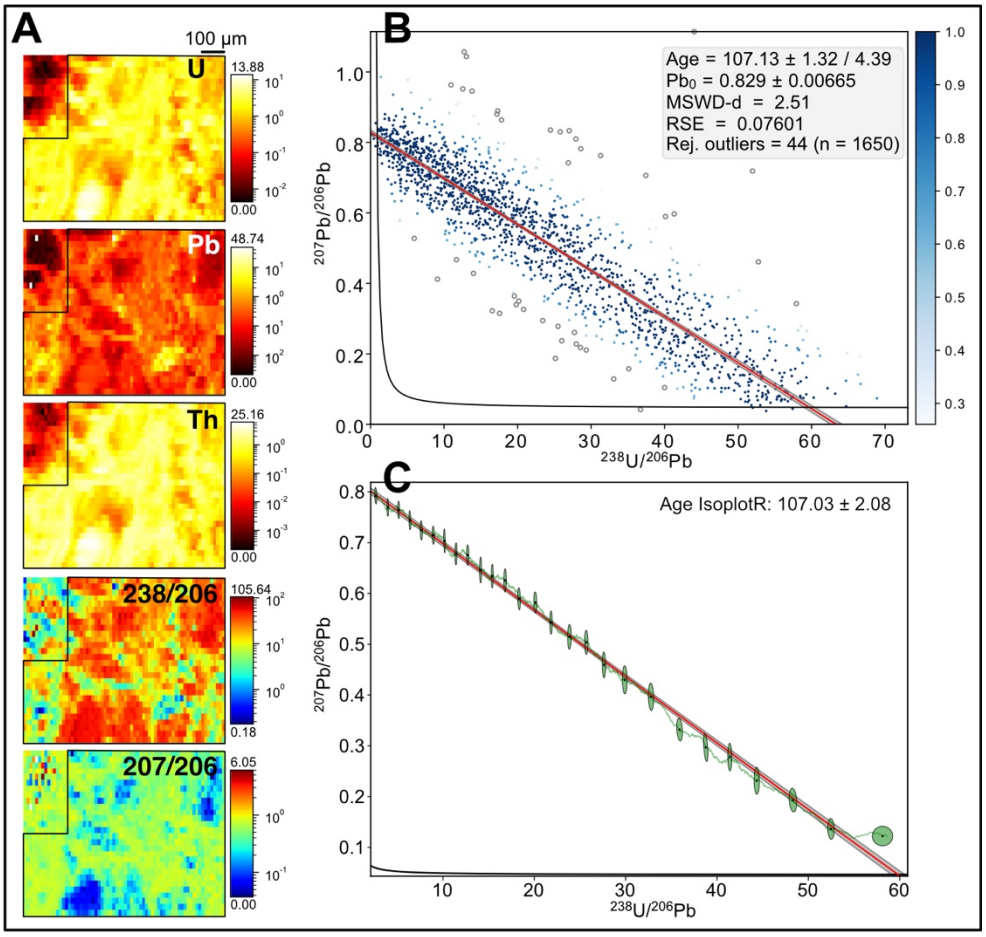

Figure 7: Results obtained for sample ARB. A: Semi-quantitative element concentrations in ppm (U, Pb, Th) and $^{238}U/^{206}Pb$, $^{207}Pb/^{206}Pb$ isotopic maps. B: TW concordia plot with ages and their uncertainty calculated by robust regression. C: TW concordia plot with pseudo-ellipses used for calculation of the d-MSWD. Age and associated uncertainty obtained by York-type regression using IsoplotR are also indicated. The pixels outside the black frames on isotopic maps (A) were not considered in age calculation, based on the colocalization study.